Appl. Phys. A (2016) 122:889
DOI 10.1007/s00339-016-0425-9

Applied Physics A
Materials Science & Processing

Optical and electrical properties of hydrothermally prepared CdTe nanowires

N. M. A. Hadia[1] · M. A. Awad[1] · S. H. Mohamed[1] · E. M. M. Ibrahim[1]

Received: 15 May 2016 / Accepted: 7 September 2016 / Published online: 14 September 2016

Abstract The hydrothermal process was used to synthesize CdTe nanowires (NWs). Various analytical techniques were used to characterize the obtained NWs. The wire diameters were in the range 35–60 nm, and the lengths were >5 μm. The CdTe NWs had zinc-blende crystal structure. The NWs had high uniformity and high yield. FTIR analysis revealed the presence of the characteristic vibrational spectra of oxygen and hydrogen bounded to Cd and Te in CdTe NWs. The optical band gap value was 2.09 eV. The CdTe NWs showed a strong red emission band centered around 620.3 nm. The conductivity measurements were carried out in the temperature range 300–500 K and in air atmosphere. Two types of conduction mechanisms were observed with activation energies of 0.27 and 0.17 eV at high and low temperature regions, respectively. These results validate the potential of CdTe NWs for optoelectronic applications.

1 Introduction

CdTe has high optical absorption coefficient in the visible spectrum with direct band gap of 1.44 eV at room temperature [1]. These characteristics made CdTe an ideal substance for photovoltaic applications. Furthermore, CdTe nanomaterials have found important applications in numerous topological fields such as light emitting diodes, biomedical applications, lasers and solar cells [2–5]. Recently, extensive studies concerning zero-dimensional (0D) and one-dimensional (1D) CdTe materials have been carried out. By controlling the morphological parameters of CdTe nanowires (NWs) or nanoparticles down to few nanometers, they can offer a wide range of band gap energies in the visible spectrum which can be ascribed to the quantum confinement effect [6, 7].

Moreover, CdTe NWs arrays with axial or radial p–n junctions are being examined as an alternative to CdTe and CdS thin films for solar cells applications. In principle, the wire arrays can offer more pronounced photon absorption in the absorber material and also more effective carrier collection [8]. CdTe NWs have been frequently prepared using various methods such as laser ablation pulsed laser deposition, template-directed electrodeposition method, vapor–liquid–solid (VLS) mechanism, solution-based growth, electrochemical synthesis, chemical vapor deposition, hydrothermal methods and closed space sublimation methods [2, 9–11]. The hydrothermal technique is vital process because it is a reproducible and it is highly scalable. Thereby, it gives reproducible results, and thus, it increases the efficiency of the prepared material. In this work, CdTe NWs are prepared by hydrothermal method, and the morphology, structure, optical, electrical and the photoluminescence (PL) properties of the products are studied for possible use in optoelectronics.

2 Experimental

2.1 Materials and synthesis procedure

Cetyltrimethylammonium bromide (CTAB; $C_{19}H_{42}BrN$), ascorbic acid ($C_6H_8O_6$), Na_2TeO_3 and $Cd(NO_3)_2{\cdot}4H_2O$ produced by Sigma-Aldrich were used without further

✉ M. A. Awad
arwamadeha@yahoo.com

[1] Physics Department, Faculty of Science, Sohag University, Sohâg 82524, Egypt

purification. In addition, double distilled water was used during the preparations. Firstly, 0.3 g of cetyltrimethylammonium bromide (CTAB) and 2.5 g of ascorbic acid ($C_6H_8O_6$) were dissolved in 40 mL of double deionized water. A mild magnetic stirring was thoroughly used for 45 min at room temperature. Secondly, 0.42 g of Na_2TeO_3 and 0.58 g of $Cd(NO_3)_2{\cdot}4H_2O$ were added to the previous solution in order. After the addition of the Na_2TeO_3, a white TeO_2 was precipitated directly. Lastly, 40 mL of double deionized water was added to the above solution under continuous stirring. The final solution was put in Teflon-lined stainless steel autoclave (100 mL in size). Then, the autoclave was sealed and maintained at 200 °C for 15 h in an electric furnace. After that the furnace was cooled to room temperature. Then, the collected products were washed in distilled water for three times and with ethanol for another three times. Finally, the products were dried in vacuum oven at 60 °C for 10 h.

2.2 Samples characterizations

To examine the structure of the samples, X-ray powder diffraction (XRD) was used. The machine was Philips X'Pert PRO MPD (PANalytical, The Netherlands) with graphite-monochromatized CuK_α radiation ($\lambda = 1.54184$ Å). It was operated at 40 mA and 45 kV. The XRD patterns were measured from 20° to 80° using θ–2θ scan.

A field emission scanning electron microscopy (FESEM) was employed to examine the morphology of the samples. The examinations were carried out using a JSM-6100 microscope (JEOL, Japan) at 30 kV acceleration voltage. An energy dispersive analysis of X-ray (EDAX) unit equipped with the FESEM was used to determine the chemical composition of the prepared nanostructures. Images of transmission electron microscopy (TEM) and the selected area electron diffraction (SAED) patterns were achieved with a 2000 EX II microscope (JEOL, Japan). The patterns were obtained at an acceleration voltage of 200 kV. A JEM-2100F (JEOL, Japan) high-resolution transmission electron micrographs (HRTEMs) with an accelerating voltage of 200 kV were used to further optimize the analysis. In order to carry out TEM analysis, the obtained products were ultrasonically dispersed in ethanol. Then, a drop of the suspension was located on a carbon coated Cu grid.

FTIR measurements were done for CdTe powder mixed with KBr. A Fourier transformation infrared spectrophotometer (IRPrestige-21, SHIMADZU) was employed to carry out the FTIR measurements in the wavenumber range 400–4000 cm^{-1}. The measurements were taken with 4 cm^{-1} resolution and at room temperature. The optical absorption spectrum was measured using the Perkin-Elmer Lambda 900 UV–Vis–NIR Spectrophotometers at room temperature. Measurements of photoluminescence (PL) were taken by using a 337 nm ILGI 503 N_2 laser. The electrical properties were studied using the two-prop method in the temperature range 300–550 K.

3 Results and discussion

3.1 Morphological and structural characteristics

Figure 1a, b shows FESEM images with low and high magnifications of CdTe sample. The sample has nanowires morphology with diameters in the range from 35 to 60 nm and the lengths >5 μm. The NWs are of high uniformity and yield. Figure 2a, b shows TEM images with low and high magnifications of CdTe NWs. Clearly, the NWs have smooth surfaces and uniform thickness along the nanowire

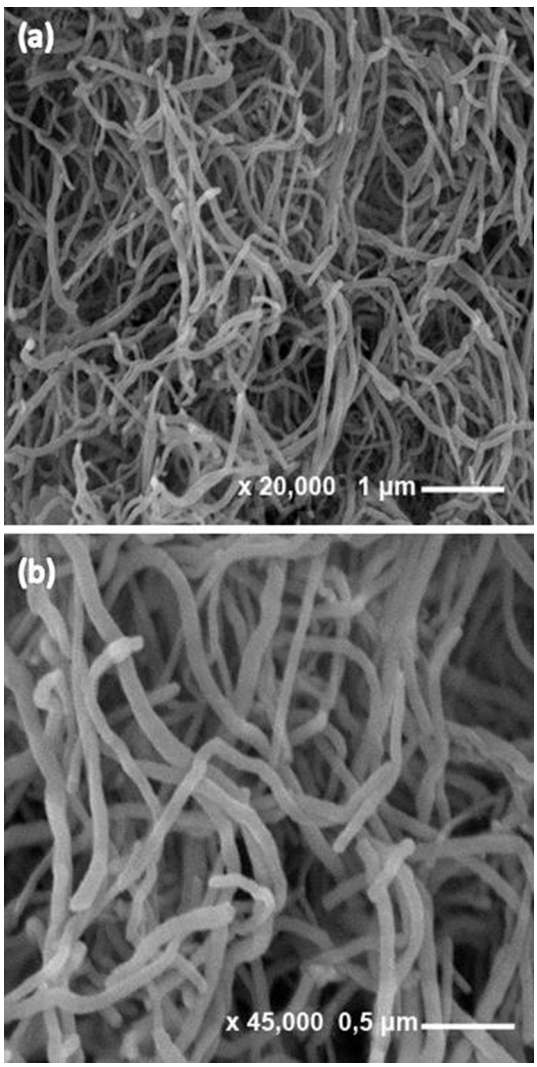

Fig. 1 FESEM images with low (**a**) and high (**b**) magnifications of CdTe sample

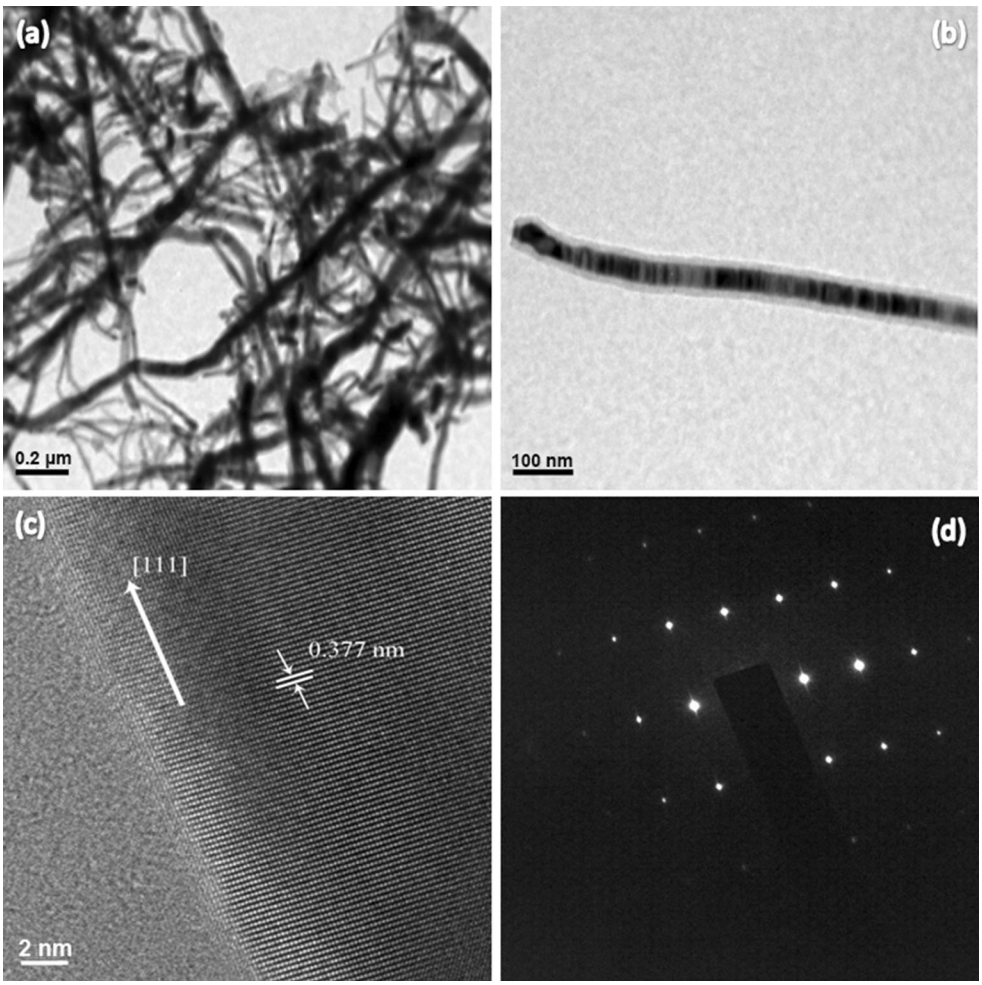

Fig. 2 **a**, **b** HRTEM image with low and high magnifications of CdTe NWs, **c** single nanowire lattice fringe separation and **d** selected area electron diffraction (SAED) pattern

axis. Figure 2c shows a high-resolution transmission electron microscope (HRTEM) image of a single CdTe nanowire. The inter-planar distance is determined to be 0.377 nm and is corresponding to the <111> direction in zinc-blende CdTe. Figure 2d displays selected area electron diffraction (SAED) pattern of CdTe NWs, verifying the single crystalline nature. The pattern can be indexed to the zinc-blende structure CdTe with growth direction along <111>.

The EDAX spectrum of CdTe sample coated with Au is shown in Fig. 3. The spectrum reveals the presence of Au, Cd and Te peaks. The Au peaks originated from the Au coating. The NWs are composed of Cd and Te with atomic percentages of 50.02 and 49.98 which are in good agreement with the stoichiometric ratio in CdTe. The additional two peaks correspond to C and O which may be attributed to the contamination from the ambient atmosphere.

The FTIR spectrum CdTe NWs are shown in Fig. 4. The band at 3721 cm^{-1} is assigned to water stretching vibrations, and the strong-broad absorption band at 3421 cm^{-1}

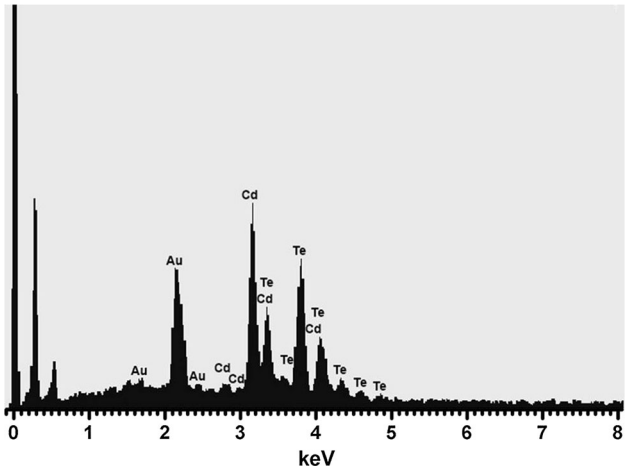

Fig. 3 EDAX spectrum of the as-prepared CdTe product

is due to O–H stretching vibration of the absorbed water on the CdTe surface. The absorption bands at 2922 and 2850 cm^{-1} are derived from the asymmetric and

symmetric stretching vibrational modes of CH_2, respectively. The absorption bands at 1685 and 1608 cm^{-1} may be derived from C=O asymmetric stretching vibrational modes [12]. The absorption bands at 1441 and 1340 cm^{-1} are tentatively assigned to C–O–H bending and C–O stretches vibrational modes [13]. The bands at 1287 and 1191 cm^{-1} may be probably ascribed to hydrogen compounds such as H–OH vibrations, while the bands in the frequency range between 996 and 400 cm^{-1} are attributed to the vibrational contributions of symmetric and asymmetric stretching oxygen compounds with Cd and Te [14].

Figure 5 shows the X-ray diffraction (XRD) pattern of typical CdTe nanowires. The pattern in Fig. 2 reveals the presence of several peaks at 23.84°, 39.38°, 46.50°, 56.76°, 62.52°, 71.22° and 76.23°. These peaks can be indexed as zinc-blende-structured CdTe (JCPDS card No. 65-8879). The lattice constant calculated from the (111) peak is $a = 0.653$ nm. This value is comparable to the value, 0.6482 nm, reported by Ebina and Takahashi [15] for unstrained CdTe lattice. No peaks due to any other phases were detected, indicating the high purity in the phase nature of the products. Strong peaks also confirm the high crystallinity of the sample.

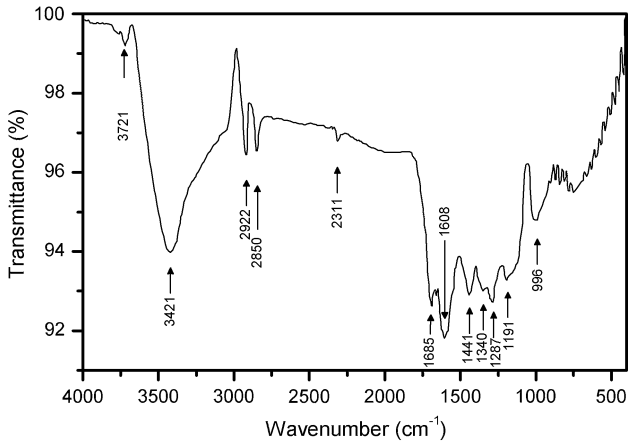

Fig. 4 FTIR transmittance spectrum of CdS NWs

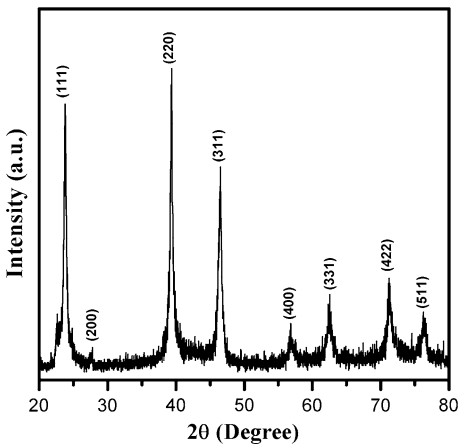

Fig. 5 XRD pattern of CdTe NWs

3.2 Optical properties

The optical absorption spectrum of CdTe nanowires is shown in Fig. 6a. The spectrum reveals that the CdTe nanowires have low absorption in the NIR region, whereas the absorption is high in the UV–Vis regions. An absorption maximum is observed at 593.5 nm which corresponds to the optical band gap. The variation in the absorption coefficient as a function of photon energy for allowed direct transitions is given by:

$$(\alpha h\nu) = A\left(h\nu - E_g\right)^{\frac{1}{2}} \quad (1)$$

where A is a constant, h is Planck's constant, ν is the frequency, and E_g is the band gap energy. The E_g value is obtained by extrapolating the linear part to intercept with the energy axis (Fig. 6b) and is found to be 2.09 eV. This value is higher than the bulk value (1.51 eV [16]) and, however, is close to the values of 2.07–2.38 eV for CdTe nanocrystals [17].

The photoluminescence of nanomaterial is complicated because it is sensitive to the preparation conditions, crystal size and shape [18]. Figure 7 gives a room temperature photoluminescence (PL) spectrum of CdTe NWs. A strong PL band appears at about 620.3 nm, which is probably a band-to-band emission as the diameter of CdTe NWs (35–60 nm) is much larger than the diameter of the Bohr exciton in bulk CdTe (10 nm) [19].

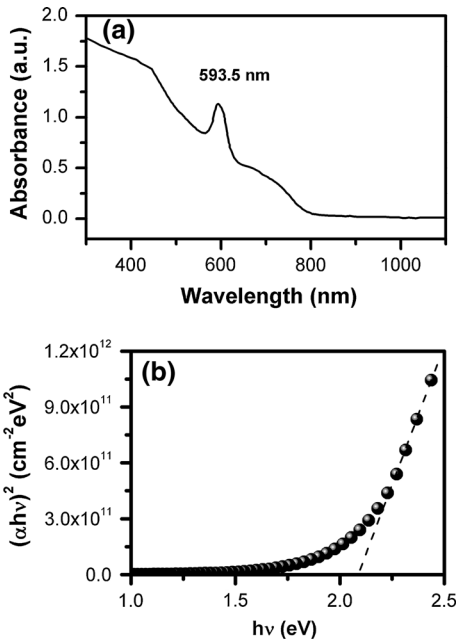

Fig. 6 Optical absorption spectrum of CdTe NWs (**a**) and $(\alpha h\nu)^2$ versus $h\nu$ plot (**b**)

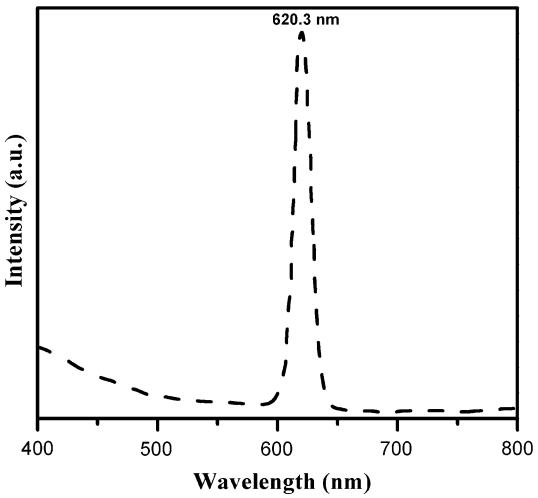

Fig. 7 Room temperature PL emission spectra of the CdTe NWs

3.3 Electrical properties

The FESEM investigation demonstrates that the conducting NWs are in close proximity. Consequently, the flowing current, between NWs, requires the electrons to jump the gaps between the NWs which can take place by hopping or tunneling [20]. Thus, to explain the conduction mechanism of CdTe NWs, the proposed model by Wuelfing and Murray [21], for thin films, may be helpful. The model describes the dependence of electrical conductivity (σ) on the average inter-nanowire distance x and the temperature (T). Also, the model suggests an Arrhenius type activated tunneling through the equation:

$$\sigma(x,T) = \sigma_0 e^{-\beta x} e^{\frac{-E_A}{KT}} \quad (2)$$

where K, E_A and β are the Boltzmann constant, the activation energy and the electron tunneling coefficient, respectively. It is obvious from Eq. 2 that the tunneling probability decreases exponentially with inter-nanowire distances [20].

The dependence of the electrical conductivity on temperature of CdTe NWs was studied in the temperature range 300–550 K. It was found that the electrical conductivity increased with the increasing temperature. This confirms that CdTe NWs has semiconducting behavior. Figure 8 shows the variation of ln σ with 1000/T. Two linear parts with different slopes can be clearly distinguished. Thermally activation natures of the conduction in the two parts are obtained which are by the linear behavior. It is seen that the transition between the two parts is not sharp, and the passage between them occurs nearly at 408.1 K. It is worth noting that the same behavior was reported for other CdTe nanostructures [21–24]. The activation energies correspond to the high (300 K $\leq T \leq$ 408.1 K) and low (408.1 K $\leq T \leq$ 500 K) temperature regions are denoted as E_{HA} and E_{LA} (see

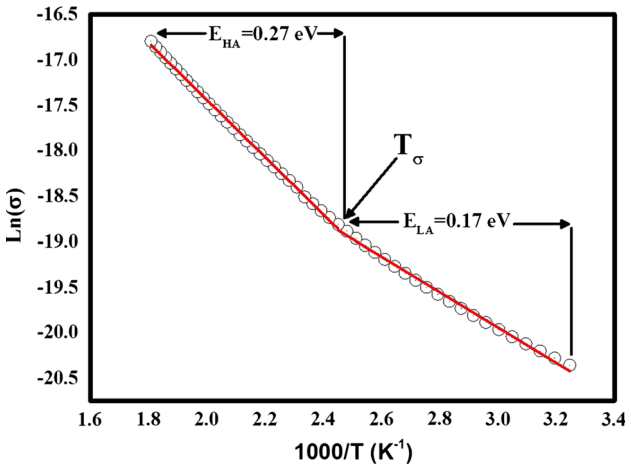

Fig. 8 Variation of ln(σ) versus 1000/T of CdTe NWs

Fig. 8). The evaluated E_{HA} and E_{LA} are found to be 0.27 and 0.17 eV, respectively. Noteworthy, the low temperature region activation energy E_{LA} is much higher than that reported by Abd El-sadek et al. ($E_{LA} = 0.069$ eV) [22]. As for the value of E_{HA}, it is slightly higher than the values reported in other works such as Ubale et al. ($E_{LA} = 0.215$ eV) [25], Abd El-sadek et al. ($E_{LA} = 0.207$ eV) [22], and it is higher than double of the value reported by Kavitha and Sakthivel ($E_{LA} \sim 1.2$ eV) [23]. This difference is realistic because the electronic transport properties of CdTe nanostructures depend considerably on several factors such as the lattice defects, crystallite shape and size, type and content of the impurities, adsorbed and absorbed gasses, etc. The low values of the electrical activation energy in comparison with the optical energy gap of the CdTe NWs can be understood in the view point of the carrier trapping model [26–28]. Based on this model, the dopants (if found) and the defects immobilized and trapped at the grain boundaries play a major role in the material in particular if the material comprises of small crystallites where the grain boundaries content becomes considerably high. In such case, substantial space near the grain boundary is charge depleted. This causes a formation of activation energy barrier across the grain boundary. The width and height of the activation energy barrier become shorter when the carriers trap in the grain boundaries are lesser as the creation of mobile defects, and then the conduction is inspired through thermionic emission [29, 30].

4 Conclusion

CdTe NWs have successfully synthesized using hydrothermal method. XRD revealed that the product is single crystalline CdTe with zinc-blende crystal structure. SEM and TEM examinations revealed that the product was

nanowires in shape. FTIR spectrum indicated peaks in the 996–400 cm^{-1} frequency range which are the superposition of the vibrational contributions of oxygen compounds. The evaluated optical band gap value was 2.09 eV. A strong red emission band centered at about 620.3 nm was observed from the PL measurements. The conductivity analysis revealed that two types of conduction mechanisms were present with activation energies of 0.27 and 0.17 eV at high and low temperature regions, respectively. The CdTe NWs could be promising in many applications such as building blocks for optoelectronics.

References

1. K. Mitchell, A.L. Fahrenbruch, R.H. Bube, J. Appl. Phys. **48**, 829 (1977)
2. W.P.R. Liyanage, J.S. Wilson, E.C. Kinzel, B.K. Durant, M. Nath, Sol. Energy Mater. Sol. Cells **133**, 260 (2015)
3. X. Li, X. Yang, L. Yuwen, W. Yang, L. Weng, Z. Teng, L. Wang, Biomaterials (2016). doi:10.1016/j.biomaterials.2016.04.014. **(in press)**
4. S. Ebrahim, M. Reda, A. Hussien, D. Zayed, Spectrochim. Acta A **150**, 212 (2015)
5. S. Chander, M.S. Dhaka, Phys. E **76**, 52 (2016)
6. A.L. Rogach, L. Katsikas, A. Kornowski, D.S. Su, A. Eychmuller, H. Weller, Ber. Bunsenges. Phys. Chem. **100**, 1772 (1996)
7. S. Patra, S.K. Pradhan, Acta Mater. **60**, 131 (2012)
8. H. Dang, V. Singh, S. Rajaputra, S. Guduru, J. Chen, B. Nadimpally, Sol. Energy Mater. Sol. Cells **126**, 184 (2014)
9. S. Liu, W.-H. Zhang, C. Li, J. Cryst. Growth **336**, 94–100 (2011)
10. S.-M. Yong, P. Muralidharan, S.H. Jo, D.K. Kim, Mater. Lett. **64**, 1551 (2010)
11. M. Shaygan, K. Davami, N. Kheirabi, C.K. Baek, G. Cuniberti, M. Meyyappan, J.-S. Lee, Phys. Chem. Chem. Phys. **16**, 22687 (2014)
12. Y. Wang, S. Liu, J. Chil. Chem. Soc. **57**, 1109 (2012)
13. K. Hoppe, E. Geidel, H. Weller, A. Eychmüller, Phys. Chem. Chem. Phys. **4**, 1704 (2002)
14. J. Polit, A. Kisiel, A. Mycielski, A. Marcelli, E. Sheregii, J. Cebulski, M. Piccinini, M. Cestelli Guidi, B.V. Robouch, A. Nucara, Phys. Stat. Sol. (c) **2**, 1147 (2005)
15. A. Ebina, T. Takahashi, J. Cryst. Growth **59**, 51–64 (1982)
16. G. Fonthal, L. Tirado-Mejia, J.I. Marin-Hurtado, H. Ariza-Calderon, J.G. Mendoza-Alvarez, J. Phys. Chem. Solids **61**, 579 (2000)
17. F. Semendy, G. Jaganathan, N. Dhar, S. Trivedi, I. Bhat, Y. Chen, Proc. SPIE **7039**, 70391L-1 (2008)
18. Y. Xia, P. Yang, Y. Sun, Y. Wu, B. Mayers, B. Gates, Y. Yin, F. Kim, H. Yan, Adv. Mater. **15**, 353 (2003)
19. G.J. Khatei, Soft Nanosci. Lett. **4**, 69 (2014)
20. K. Sharma, A.S. Al-Kabbi, G.S.S. Saini, S.K. Tripathi, Appl. Phys. A **108**, 911 (2012)
21. W.P. Wuelfing, R.W. Murray, J. Phys. Chem. B **106**, 3139 (2002)
22. M.S. Abd El-sadeka, I.S. Yahiab, A.M. Salemd, Mater. Chem. Phys. **130**, 591 (2011)
23. R. Kavitha, K. Sakthivel, Superlattices Microstruct. **86**, 51 (2015)
24. S. Singh, R. Kumar, K.N. Sood, Thin Solid Films **519**, 1078 (2010)
25. A.U. Ubale, R.J. Dhokne, P.S. Chikhlikar, V.S. Sangawar, D.K. Kulkarni, Bull. Mater. Sci. **29**, 165–168 (2006)
26. M.M. Mandurah, K.C. Saraswat, T.I. Kamins, I.E.E.E. Trans, Electron Dev. **28**, 1163 (1981)
27. M.M. Mandurah, K.C. Saraswat, T.I. Kamins, I.E.E.E. Trans, Electron Dev. **28**, 1171 (1981)
28. J. Levinson, J. Appl. Phys. **53**, 1193 (1982)
29. R.S.S. Saravanan, D. Pukazhselvan, C.K. Mahadevan, J. Alloys Compd. **517**, 139 (2012)
30. V. Šnejdar, J. Jerhot, Thin Solid Films **37**, 303 (1976)